Journal of Nuclear Materials 440 (2013) 586–595

Contents lists available at SciVerse ScienceDirect

Journal of Nuclear Materials

journal homepage: www.elsevier.com/locate/jnucmat

Presented at the NuMat 2012 Conference, 22–25 October 2012, Osaka, Japan

Effect of thermo-mechanical cycling on zirconium hydride reorientation studied in situ with synchrotron X-ray diffraction

Kimberly B. Colas [a,*], Arthur T. Motta [a], Mark R. Daymond [b], Jonathan D. Almer [c]

[a] Department of Mechanical and Nuclear Engineering, Penn State University, University Park, PA 16802, USA
[b] Department of Mechanical and Materials Engineering, Queen's University, Kingston, ON, Canada K7L 3N6
[c] Advanced Photon Source, Argonne National Laboratory, Argonne, IL 60439, USA

ARTICLE INFO

Article history:
Available online 24 April 2013

ABSTRACT

The circumferential hydrides normally present in nuclear reactor fuel cladding after reactor exposure may dissolve during drying for dry storage and re-precipitate when cooled under load into a more radial orientation, which could embrittle the fuel cladding. It is necessary to study the rates and conditions under which hydride reorientation may happen in order to assess fuel integrity in dry storage.

The objective of this work is to study the effect of applied stress and thermal cycling on the hydride morphology in cold-worked stress-relieved Zircaloy-4 by combining conventional metallography and in situ X-ray diffraction techniques. Metallography is used to study the evolution of hydride morphology after several thermo-mechanical cycles. In situ X-ray diffraction performed at the Advanced Photon Source synchrotron provides real-time information on the process of hydride dissolution and precipitation under stress during several thermal cycles. The detailed study of diffracted intensity, peak position and full-width at half-maximum provides information on precipitation kinetics, elastic strains and other characteristics of the hydride precipitation process.

The results show that thermo-mechanical cycling significantly increases the radial hydride fraction as well as the hydride length and connectivity. The radial hydrides are observed to precipitate at a lower temperature than circumferential hydrides. Variations in the magnitude and range of hydride strains due to reorientation and cycling have also been observed. These results are discussed in light of existing models and experiments on hydride reorientation. The study of hydride elastic strains during precipitation shows marked differences between circumferential and radial hydrides, which can be used to investigate the reorientation process.

1. Introduction

During operation in a Light-Water Reactor (LWR), the zirconium fuel cladding absorbs hydrogen formed by the corrosion reaction as well as by water radiolysis and other sources. Due to its low solubility limit in zirconium, hydrogen atoms precipitate as zirconium hydrides [1]. Typically in LWR conditions, face-centered cubic delta hydride platelets are formed ($ZrH_{\sim 1.66}$). The orientation and shape of the hydride platelets is strongly dependent on the texture and thermal history of the material [2]. In typical fuel cladding, hydride platelets precipitate preferentially in the circumferential orientation (platelet surface in the circumferential–axial plane of the cladding tube).

After operation in the core of a nuclear power plant, the used nuclear fuel is stored in spent fuel pools for a certain number of years until the decay heat is reduced. After this period, the spent fuel can be dried out and placed in dry storage. Several drying processes exist, the most extreme of which is vacuum drying, which consists of heating the fuel rods to 400 °C for a short time, followed by cool-down, repeating the procedure up to nine times to ensure the removal of water. The temperature increase raises the rod internal pressure from fission gases produced during operation, applying a tensile hoop and axial stress to the cladding tube. At the beginning of dry storage, the cladding temperature is typically about 300 °C, slowly decreasing during the following years [3,4]. The hoop stresses in the fuel cladding are about 35–65 MPa when the fuel is in the spent fuel pool cool-down and 70–150 MPa during drying operation and storage (with axial stress approximately half the hoop stress) [3]. Hydride reorientation can occur when the hydrogen in solid solution precipitates as the cladding is cooled from elevated temperatures under stress. As the hydride platelets precipitate under an applied hoop stress, they tend to reorient themselves perpendicular to the applied tensile load, thus becoming radial hydrides [2,5], which can significantly degrade the cladding ductility [6].

* Corresponding author. Present address: CEA-Saclay, French Atomic Energy Commission, DEN/DANS/DMN/SEMI/LM2E, 91191 Gif-sur-Yvette Cedex, France. Tel.: +33 1 69 08 18 42; fax: +33 69 08 90 73.
E-mail address: kimberly.colas@cea.fr (K.B. Colas).

0022-3115/$ - see front matter © 2013 Elsevier B.V. All rights reserved.
http://dx.doi.org/10.1016/j.jnucmat.2013.04.047

Previous studies on hydride reorientation performed with conventional metallography have provided important information on the threshold stresses for reorientation and on the factors that influence it. However, because these studies are performed post-facto they can only access the final state of the material and no direct study of precipitation mechanisms can be made. Recent in situ synchrotron experiments have shown the potential to study in situ hydride dissolution and precipitation with and without applied stress [7,8]. Hydride and zirconium strains were also followed in situ in samples with a stress concentration [9,10]. These in situ X-ray diffraction techniques are used in this article and combined with conventional metallography to study the mechanisms of reoriented hydride nucleation and growth. The hydride volume fraction, phase and strain states are followed during dissolution and precipitation during several thermo-mechanical cycles. In particular, the effect of cycling on the evolution of hydride strains, orientation and microstructure is investigated.

2. Experimental procedures

2.1. Material and sample preparation

The material used in this study is cold-worked Zircaloy-4 sheet, 675 μm thick, furnished by Teledyne Wah-Chang. The as-received sheet was stress-relieved for 2 h at 510 °C under vacuum of 10^{-3} Pa, resulting in a cold-worked stress-relieved (CWSR) state. The microstructure, texture and mechanical properties of this material are typical of textured sheet and are described in more detail in [11]. The zirconium grains are elongated in the rolling direction with an average grain size of 6 μm × 4.5 μm × 2.5 μm. Pole figures indicated that the basal poles were tilted by 30° on average away from the normal direction in the transverse direction and that one of the prism directions was aligned with the rolling direction as expected. The Kearns factors (the resolved fractions of basal poles aligned with each macroscopic direction) were measured by the direct and inverse pole figure methods to be equal to 0.59 in the normal/radial direction, 0.30 in the transverse/circumferential direction and 0.14 in the rolling/axial direction [11]. This texture is similar to that measured in CWSR zirconium cladding [12]. The yield stress of this material tested at several temperatures is 5–10% lower than that of cladding tube [11].

The samples were then hydrided by gaseous charging as described in [7]. This technique starts by removal of the native oxide layer by acid etching followed by deposition of a thin nickel layer to act as a window for hydrogen atoms and to prevent oxidation. After this step, the samples are heated to 450 °C in a volume filled with a mixture of 88% argon and 12% hydrogen for 1 h until the hydrogen is absorbed, then furnace cooled. The hydrogen content in the material is tested using hot vacuum extraction. The hydrogen contents for the samples studied were between 190 and 350 wt.ppm.

Once the samples are hydrided, they are machined as small dogbone-shaped tensile specimens. The specific dimensions of the specimens are presented in [13]. It is important to note that the transverse direction (TD) lies along the sample gage section. The rolling direction (RD) is perpendicular to the gage section in the plane of the tensile specimen. The normal direction (ND) is perpendicular to the plane of the tensile specimen. The ND corresponds to the radial direction in a tube, the RD to the axial direction and the TD to the circumferential direction. Thus in-plane hydrides in our sheet material are called circumferential hydrides and out-of-plane hydrides are called radial hydrides.

2.2. Metallography

Metallography is performed on the samples in order to observe the hydride microstructure. The samples are mounted in epoxy casts, polished to 1200 grit silicon carbide paper then etched for a few seconds in a solution of one volumetric part HF, 10 parts nitric acid and 10 parts H_2O. Prior to any thermo-mechanical treatment, a small piece of the grip section of each sample is cut off for metallographic analysis to characterize the starting microstructure of the samples. An example of such a starting microstructure for different samples is seen in the cross-sectional optical images in the upper left-hand side of Fig. 2. The hydrides are mostly circumferential (i.e. platelets in the rolling-transverse plane). This morphology has been linked to the texture of the CWSR material which presents many basal poles along the normal direction, perpendicular to the rolling-transverse plane. Hydride platelets typically precipitate perpendicular to the basal pole due to the δ-hydride{1 1 1}//α-zirconium{0 0 0 2} orientation relationship [14]. Also the presence of elongated grains makes it easier for hydrides to precipitate in the circumferential direction. After thermo-mechanical treatment, the sample microstructure is again characterized by metallography.

2.3. Thermo-mechanical treatment

Several samples with different thermo-mechanical cycles were studied. An example of such a thermo-mechanical treatment is presented in Fig. 1. The heating rate is 25 °C/min and the cooling rate is 1 °C/min. In this case, the sample was heated until all the hydrides were dissolved (i.e. above the dissolution temperature). For a sample with 192 wt.ppm of hydrogen, for example, 410 °C was the high temperature used. At that temperature, a tensile stress of 240 MPa corresponding to ~85% of the yield stress at 410 °C is applied in the transverse direction (TD). The stress is maintained at a constant value while the sample is cooled back to 150 °C. At that temperature, the stress is reduced to zero and most of the hydrogen has re-precipitated as hydrides. This constitutes one cycle. The sample shown in Fig. 1 went through four of these thermo-mechanical cycles. Various levels of stress, temperatures and number of cycles were applied to the samples with various levels of hydrogen content, as presented in this study. For the samples with 300 and 330 wt.ppm the maximum solution temperature reached during the thermo-mechanical treatment was 450 °C. The hydrogen content, number of thermo-mechanical cycles and the maximum temperature reached during each thermo-mechanical cycle are presented in the left-hand side of Table 1 for the samples studied in this work.

2.4. Synchrotron X-ray diffraction

X-ray diffraction experiments were performed at beamline 1-ID at the Advanced Photon Source synchrotron at Argonne National Laboratory. Detailed description of the transmission in situ diffraction technique and data analysis can be found in [7,15]. A 76 keV X-ray beam was used for these experiments, which allows transmission of the X-rays through the sample thickness. As a result the whole specimen thickness is sampled with a scattering volume of 200 μm × 200 μm × 600 μm (beam size horizontally × beam size vertically × sample thickness). The diffraction rings obtained are recorded onto a two-dimensional amorphous silicon detector allowing for some texture information to be measured as well as crystallographic information. Diffraction data is recorded every 30 s during heating and cooling of the sample, which allows detailed study of hydride dissolution and precipitation kinetics.

The intensity of the diffraction rings obtained are then integrated over four specific directions: ±10° around 0°, 90°, 180° and 270°. The results from 0° and 180° and 90° and 270° are then respectively added together for better statistics. Given our sample orientation, the [0°; 180°] direction corresponds to the rolling direction and the [90°; 270°] direction corresponds to the transverse direction. Families of planes perpendicular to the TD (direction of the applied stress) and perpendicular to the RD are studied in this

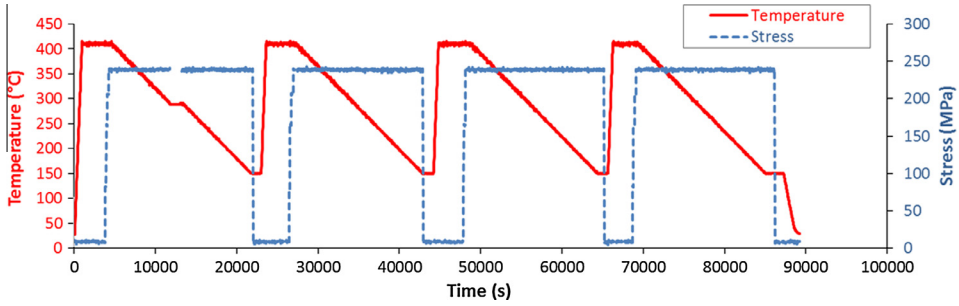

Fig. 1. Example of four thermo-mechanical cycles as applied to a sample with 192 wt.ppm of hydrogen.

Table 1
Measured and expected dissolution and precipitation temperatures for CWSR Zircaloy-4 samples cycled with and without stress. The DSC temperatures are taken from [21].

	Cycle #	[H] content (wt.ppm)	Max temp. (°C)	Heating/cooling rates (°C/min)	Measured T_p (°C)	DSC T_p (°C)	Measured T_d (°C)	DSC T_d (°C)
No stress	1	130	450	25/1	300	320	420	370
No reorientation	2	130	450	25/1	310	320	420	370
160 MPa stress	1	90	450	25/1	330	300	380	340
No reorientation	2	90	450	25/1	310	300	380	340
230 MPa stress	1	192	410	25/1	340	360	400	410
	2	192	410	25/1	335	360	390	410
Reorientation	3	192	410	25/1	340	360	390	410
	4	192	410	25/1	340	360	390	410

experiment. Once integrated the diffraction peaks are fitted using the GSAS software [16] by iterative refinement of the peaks shapes, intensities and widths. The focus of this study is on the most intense hydride peak δ{1 1 1}, and the neighboring Zr-α{10.0}. These peaks provide the greatest accurary in strain determination.

3. Results and discussion

3.1. Evolution of hydride morphology with thermo-mechanical cycling

As discussed in the introduction, the reoriented hydrides fraction can significantly degrade cladding ductility [6]. In this study, the reorientation of hydrides is quantified by the Radial Hydride Fraction (RHF) parameter using the data produced by the Hydromorph® program from CEA (French Atomic Energy Commission), which measures the percentage of hydrides that are classified as "radial" [17]. The RHF is calculated as a weighted average of hydride lengths given by the following equation:

$$\mathrm{RHF} = \frac{\sum_i L_i f_i}{\sum_i L_i} \tag{1}$$

where L_i is the length of the ith hydride and f_i is the weighting factor. Hydrides with an orientation between 0° and 40° to the transverse direction have a weight f_i of 0, hydrides with an orientation between 40° and 65° have a weight f_i of 0.5, and hydrides with an orientation of 65–90° have a weight f_i of 1. This definition for radial hydride fraction has been chosen over a definition that uses a continuous weighting function, such as sine or sine-squared. This is because slight inclinations of circumferential hydrides can provide contributions to RHF that tend to inflate the RHF values beyond what is represented in the corresponding micrographs. The numbers calculated with the present definition of RHF were found to accurately represent the type of hydride morphology, showing low percentages for microstructures composed of fully circumferential hydrides and percentages close to 90–100% for fully reoriented hydrides.

Hydride connectivity and hydride size are also crucial factors for cladding failure analysis. High hydride connectivity is reached when hydrides are inter-connected forming an nearly continuous path for a crack to propagate through the thickness of the sample. When the hydride population is highly reoriented with long highly connected hydrides, a crack can easily propagate through the thickness. It is found that number of thermal cycles and the hydrogen content influence both the radial hydride fraction and hydride size.

Fig. 2 shows the calculated RHF and hydride length plotted versus the number of thermo-mechanical cycles for a sample with 192 wt.ppm of hydrogen heated to 410 °C and cooled under an applied stress of 230 MPa. The evolution of the hydride microstructure can be seen in the optical micrographs. As more thermo-mechanical cycles are applied to the sample, the hydride morphology becomes increasingly radial. As the hydrides reorient, the hydride length initially decreases then steadily increases with increasing number of cycles. Thermal cycling also significantly increases hydride connectivity. Thus the changes in hydride morphology induced by repeated cycling can be very detrimental to cladding ductility.

Fig. 3 shows the results of samples with different hydrogen content submitted to one thermo-mechanical cycle. Samples have been taken to a temperature sufficiently high for full dissolution of hydrides (410 °C for the 230 wt.ppm sample and 450 °C for the 300 samples). It should be noted that in the case of the 330 wt.ppm sample, full dissolution of the hydrides was not achieved at the maximum temperature of 450 °C. The hydrides in the 300 wt.ppm sample appear slightly thicker than those in the 230 and 330 wt.ppm sample; this could be due to differences in the etching time of these samples to reveal the microstructure. It can be seen that for hydrogen contents above 200 wt.ppm, the radial hydride fraction decreases as a function of hydrogen content. The radial hydride content in wt.ppm however remains constant for both samples in which full dissolution was achieved (the 230 wt.ppm and

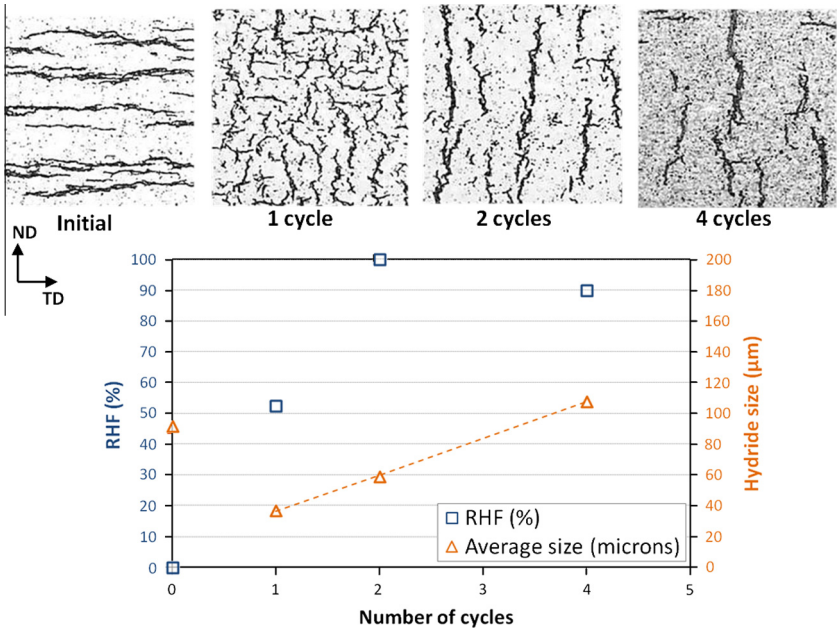

Fig. 2. Evolution of RHF and hydride size with number of thermal cycles for CWSR Zr-4 samples with 192 wt.ppm of hydrogen cooled under 230 MPa applied stress (cooled at 1 °C/min). Optical micrographs are 200 μm × 200 μm.

the 300 wt.ppm samples respectively). In these two samples, there is 117 wt.ppm of radial hydrides. This could suggest there are a limited number of sites favoring reorientation and that once they are filled, hydrides precipitate in the circumferential orientation. This could be due to a combination of several factors such as cooling rate or grain geometry for example. For the sample with 330 wt.ppm, the radial hydride content is approximately 33 wt.ppm. In this case where circumferential hydrides were still present at high temperature, it is more difficult to nucleate new radial hydrides. The hydrogen in solid solution will go preferentially to the pre-existing circumferential hydrides thus both the radial hydride fraction and the radial hydride content drastically decrease. The size of the reoriented hydride particles does not vary significantly for hydrogen contents above 200 wt.ppm.

3.2. Kinetics of hydride dissolution and precipitation

As can be seen from the previous section, thermal cycling under stress influences both hydride reorientation and the morphology of reoriented hydrides. The effect of thermal cycling on the dissolution and precipitation kinetics of hydrides studied in situ by synchrotron X-ray diffraction is presented in this section. The dissolution and precipitation temperatures can be measured by following the diffraction signal with synchrotron radiation.

The dissolution and precipitation temperatures measured for samples cycled under various levels of applied stress are summarized in Table 1. The method for the measurement of the dissolution and precipitation temperatures using the integrated hydride diffraction peak intensities has been described elsewhere [7]. It should be noted however that the measure of the dissolution temperature is less precise than that of the precipitation temperature because the heating rate is higher than the cooling rate (25 °C/min heating, 1 °C/min cooling) and thus less data points are available.

It can be seen in Table 1 that the threshold stress for hydride reorientation in the CWSR Zircaloy-4 sheet used in this study is between 160 and 200 MPa for uniaxial loading. This range of threshold stress is consistent with previous literature results for similar material and microstructure [18]. Slightly lower values were also observed for the threshold stress of hydride reorientation in the literature [6,19,20]; these differences could be due to the fact that different materials, microstructures, texture, irradiation levels and level of stress triaxiality were studied in these papers. The dissolution and precipitation temperatures do not significantly change from one thermal cycle to the next. In the absence of applied stress, the dissolution and precipitation temperatures are close to the T_d and T_p measured using DSC [21]. The absence of systematic bias in the comparison of the temperatures measured by in situ synchrotron and DSC has already been demonstrated for similar samples and experimental conditions as those presented in this study [7].

Fig. 4 shows dissolution and precipitation temperatures of a sample with 192 wt.ppm of hydrogen cycled to 410 °C and cooled

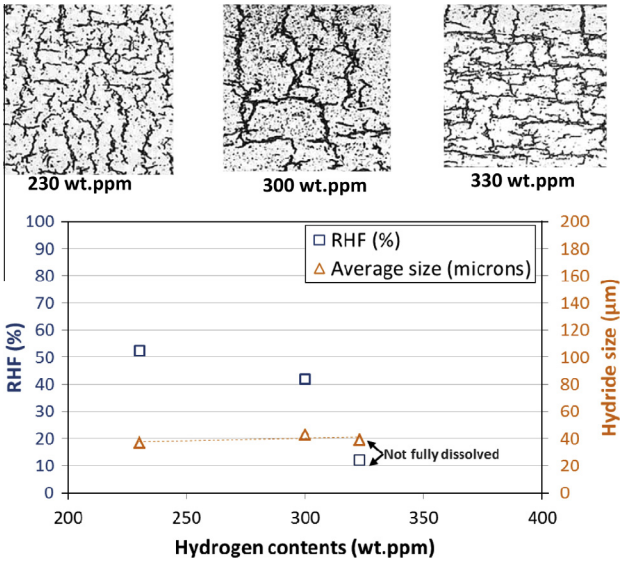

Fig. 3. Evolution of RHF and hydride size with hydrogen content for CWSR Zr-4 samples cooled under 230 MPa applied stress (1 thermal cycle, cooled at 1 °C/min). Optical micrographs are 200 μm × 200 μm. Note: full dissolution of the hydrides was not achieved at the maximum temperature of 450 °C for the 330 wt.ppm sample.

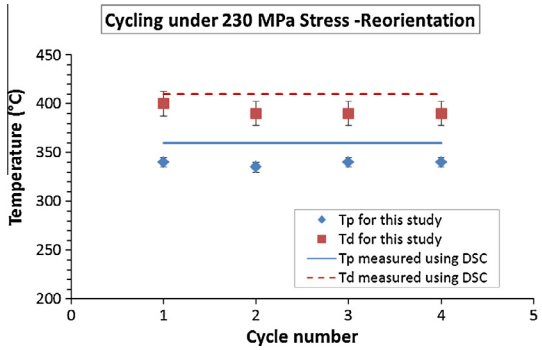

Fig. 4. Dissolution (T_d) and precipitation (T_p) temperatures of a CWSR Zr4 sample thermally cycled under 230 MPa stress (full reorientation). The expected T_d and T_p are from DSC of unstressed samples [21].

under 230 MPa stress. Both the precipitation and dissolution temperatures are constant with the number of cycles. The precipitation temperature measured by DSC for the equivalent unstressed sample [21] is higher than the measured precipitation temperature. This result means that reoriented hydrides precipitate at a lower temperature than circumferential hydrides, indicating that a greater degree of undercooling is necessary for reoriented hydrides to form. It should be added however that for samples stressed but not reoriented as seen in Table 1, the precipitation temperature is similar to that of unstressed samples. Our interpretation is that the applied stress raises the energy for precipitation in the circumferential direction, thus suppressing it, and enabling radial precipitation instead. This result is discussed in more detail in [22].

It is interesting to note that although the hydriding cycle differs in cooling rate (<0.5 °C/min) from the in situ experiments presented here (1 °C/min) the measured dissolution and precipitation temperatures are the same for all cycles. In particular, the first cycle does not differ from the subsequent ones.

The in situ recording of hydride diffraction data also allows us to follow the precipitation rate of hydrides during cool-down under different levels of applied stress and for different numbers of cycles. The precipitation rate observed in samples with hydride reorientation appears to be different from that seen in samples where circumferential hydrides precipitate (both unstressed samples and stressed but non-reoriented samples). When fitting the precipitation of hydrides in reoriented samples, two different precipitation kinetics regimes have been observed as described below.

Fig. 5 shows the amount of hydrogen in solid solution calculated by studying the evolution of the main δ{1 1 1} hydride peak intensity. From literature, the evolution of the hydrogen concentration in solid solution with temperature can be fitted to a classical exponential behavior [23]:

$$[\mathrm{H}] = A\exp(-Q/RT) \tag{2}$$

with [H] and A in wt.ppm, Q in J/mol, R = 8.314 J/mol/K and T the temperature in K. In order to obtain the [H] in solid solution, a simple subtraction has been performed:

$$[\mathrm{H}] = [\mathrm{H}]_{\mathrm{tot}}\left(1 - \frac{I(T)}{I(30\,^{\circ}\mathrm{C})}\right) \tag{3}$$

where $[\mathrm{H}]_{\mathrm{tot}}$ is the total hydrogen content in wt.ppm (measured by hot vacuum extraction), $I(T)$ is the hydride peak intensity at temperature T and $I(30\,^{\circ}\mathrm{C})$ is the hydride peak intensity at 30 °C. This equation assumes that the hydrogen solubility in Zircaloy at 30 °C is zero (in the literature, it has been found to be less than 1 wt.ppm) [8].

The parameter Q represents the activation energy for dissolution or precipitation of hydrides depending on whether the sample is heated or cooled. The value for this activation energy found for unstressed samples (24,320 J/mol) is similar to the values found in the literature for similar material from McMinn (34,469 J/mol) [24], Une (28,068 J/mol) [21] by DSC and from Zanellato (29,630 J/mol) [8] by in situ X-ray diffraction. The value of the activation energy for the stressed but not reoriented sample (Fig. 5b) is lower (12040 J/mol) than for the unstressed sample. This could mean that the applied tensile stress somewhat decreases the activation energy for precipitation of circumferential hydrides. This effect is small however given that the activation energy is estimated with a typical error of ±5000 J/mol. The activation energy for the variation of hydrogen in solid solution with temperature (and thus time, since temperature varies constantly with time) appears to be constant for unstressed samples (Fig. 5a) and samples that are stressed but not reoriented (Fig. 5b) throughout the temperature range. In contrast, for samples that exhibit hydride reorientation (cooled under 240 MPa applied stress) the activation energy for the variation of hydrogen in solid solution is higher at low temperature than at high temperature. In this case, the transition temperature is 230 °C, below which the Q value increases. In the first cycle, the difference in high temperature and low temperature Q values is less marked (40,000–53,000) than in subsequent cycles (35–50,000 to 88–100,000).

The reason for the different precipitation regimes could be as follows. When no stress is applied hydrides re-precipitate in the same circumferential or in-plane locations as before, requiring little activation energy to nucleate the new particles as they precipitate near grain boundaries, within dislocation networks left behind by the prior hydrides (which causes the hydride memory effect [25]) and in good orientation relationship. In the first cycle, stress causes hydride reorientation to start to occur, likely requiring the nucleation of new particles, which have a different activation energy from their growth. In the second to fourth cycles the greater percentage of reoriented hydrides causes this behavior to be more prevalent.

3.3. Hydride elastic strains

The study of the diffraction peak positions of the hydride δ{1 1 1} and zirconium α{10.1} gives information on the elastic strains of these two phases during dissolution and precipitation. The strain represented here is the uniaxial strain calculated using the first data point at time zero and room temperature in the following manner:

$$\varepsilon = \frac{d(\{hkl\},T) - d(\{hkl\},30\,^{\circ}\mathrm{C})}{d(\{hkl\},30\,^{\circ}\mathrm{C})} \tag{4}$$

The reference d-spacing at room temperature for the zirconium peaks comes from the first diffraction pattern recorded at room temperature, before any thermo-mechanical treatment. The reference d-spacing for the hydride strain calculation is different than the one chosen for the zirconium strain calculation and is described below. The strains measured from the shift in d-spacing of α{10.1} planes in the zirconium matrix at the fourth thermo-mechanical cycle and calculated using Eq. (4) in both TD and RD are presented respectively in Fig. 6a and 6b. (Note: the thermal schedule for all four cycles is seen in Fig. 1). The 240 MPa stress was applied in the TD during cooling. The tensile frame was operated in load control, ensuring a constant load was applied on the sample during cooling.

In Fig. 6a the lattice strain first increases as the sample is heated, due to thermal expansion. In the temperature region ~250 °C to ~390 °C an additional contribution to the strain comes from lattice expansion caused by the dissolution of hydrogen into the α-zirconium matrix. This additional contribution stops at T_d = 390 °C when all hydrides are dissolved. Once the load is applied in the TD, the lattice strain in the TD increases from 3.0×10^{-3} to 6.0×10^{-3}. Cooling then causes the d-spacing to decrease from thermal contraction and from precipitation. It is noticeable that when precipitation starts at T_p = 340 °C removing hydride from solid solution, an inflection in

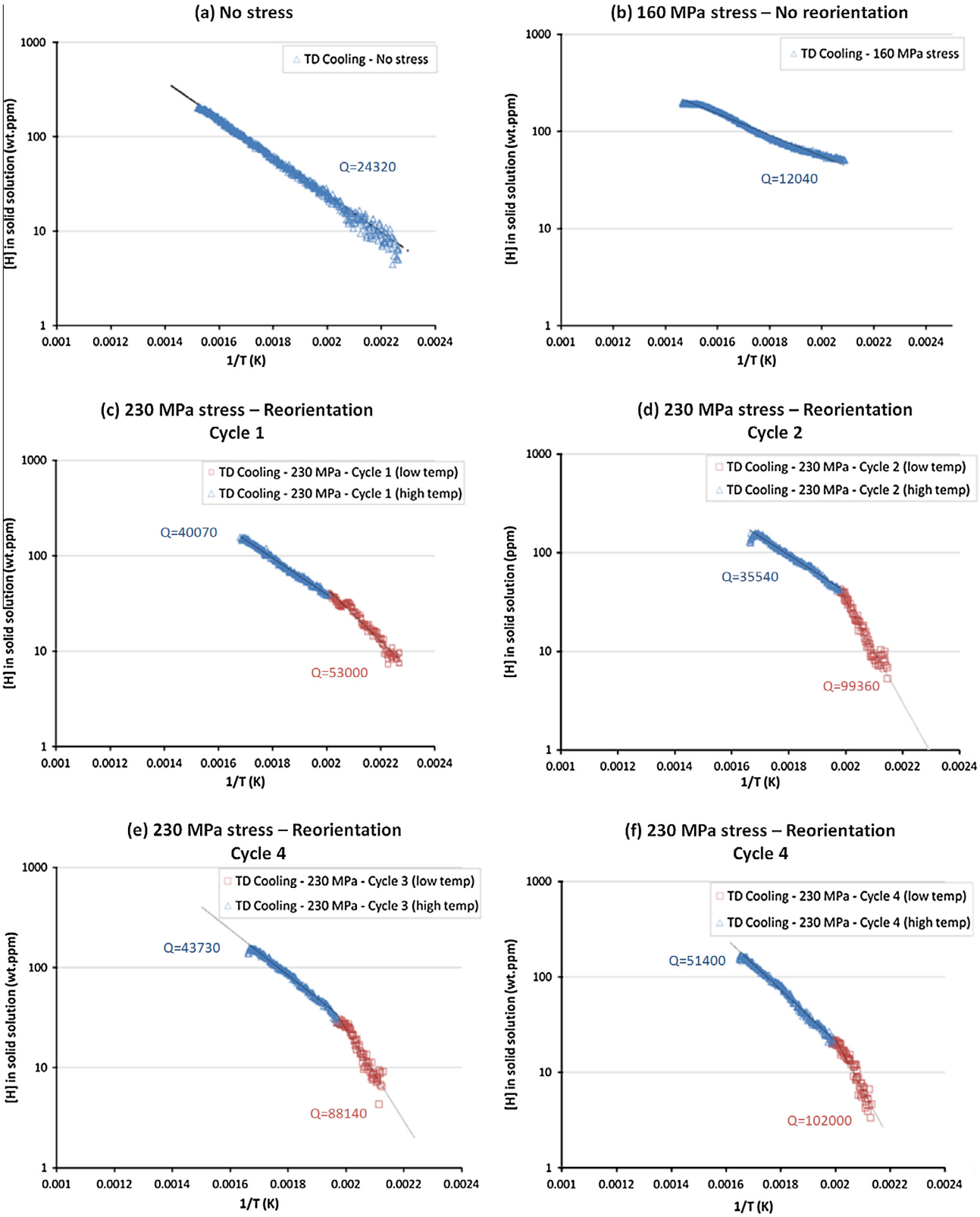

Fig. 5. Evolution of hydrogen in solid solution as a function of inverse temperature for CWSR Zr-4 samples (with 200–300 wt.ppm of hydrogen) during cooling under (a) no stress, (b) 160 MPa stress (no reorientation), (c–f) 230 MPa stress, for 1, 2, 3 and 4 thermal cycles respectively (reorientation); (integration along the transverse direction). (Note: Q is in J/mol).

the curve is obtained showing the contribution of hydrogen removal from solution to the strain decrease. At the end of the test, the load is removed and the d-spacing returns to its original value.

In Fig. 6b, the lattice strain behavior in the RD during heating is similar to that of the strain in the TD described in the previous paragraph. When the load is applied, the strain in the RD decreases

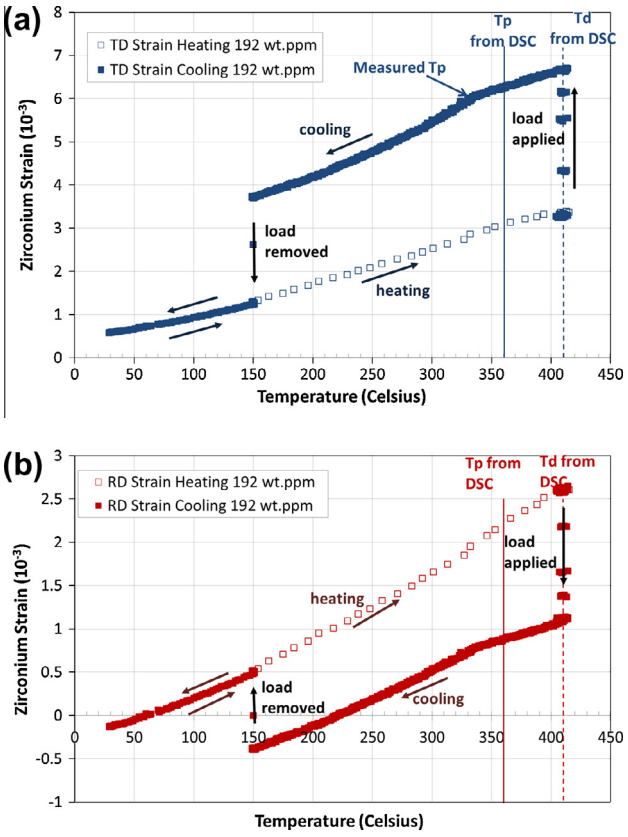

Fig. 6. Strain of zirconium (100) peak (a) in the TD and (b) in the RD in a sample with 192 wt.ppm of hydrogen cooled for the 4th cycle under a 230 MPa applied stress (stress applied in the TD, full reorientation of hydrides).

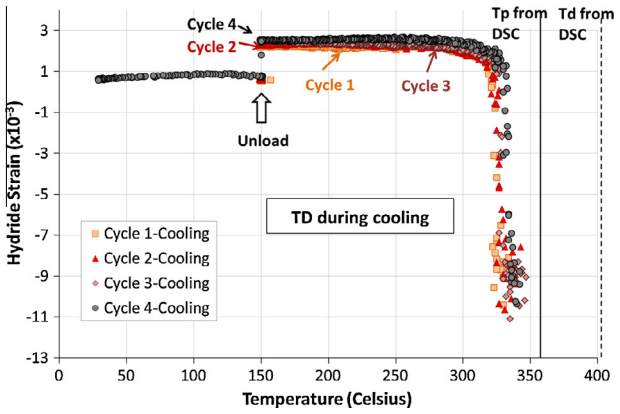

Fig. 7. Strain of hydride (111) peak in the TD in a sample with 192 wt.ppm of hydrogen during cooling for four cycles under a 230 MPa applied stress (stress applied in the TD, full reorientation of hydrides).

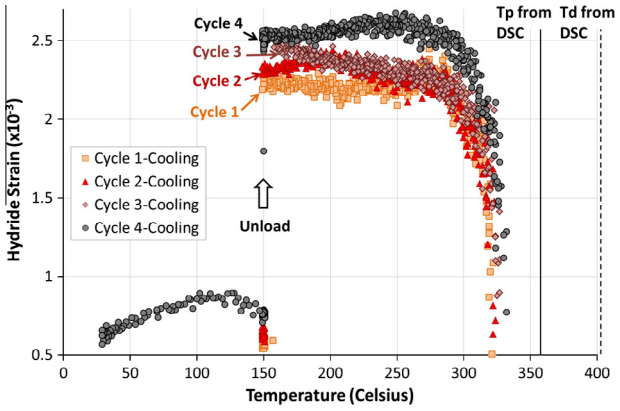

Fig. 8. Close-up of Fig. 7: Strain of hydride (111) peak in the TD in a sample with 192 wt.ppm of hydrogen during cooling for four cycles under a 230 MPa applied stress (stress applied in the TD, full reorientation of hydrides).

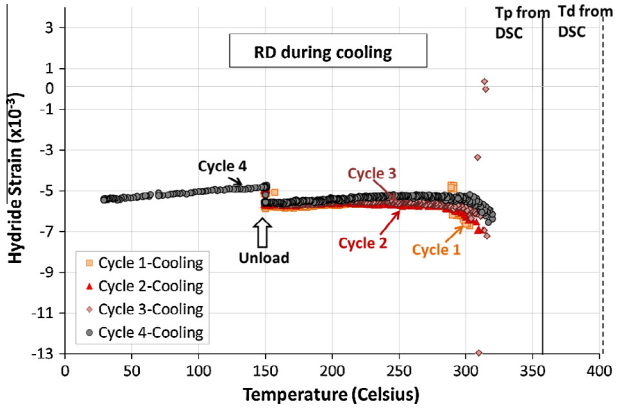

Fig. 9. Strain of hydride (111) peak in the RD in a sample with 192 wt.ppm of hydrogen during cooling for four cycles under a 230 MPa applied stress (stress applied in the TD, full reorientation of hydrides).

due to Poisson's effect (contraction of the planes perpendicular to the tensile direction). Upon cool-down the strain decreases and inflections in the curve for the strain in the RD are similar to those described in the previous paragraph for the strain in the TD.

The strains in the zirconium matrix for cycles 1, 2 and 3 were also analyzed and are similar to those in cycle 4. The study of these zirconium strains gives a reference for the study of the hydride strains.

Fig. 7 shows the strains in hydrides measured from the shift in *d*-spacing of the δ{111} planes oriented in the TD during the cool-down and hydride precipitation phase for all four cycles. These *d*-spacings can be associated with strains calculated using Eq. (4) with the hydride reference value taken as the value at high temperature just before hydride dissolution (which is close to the unstressed *d*-spacing of bulk hydrides from literature calculated at that temperature [26]). A close-up of these strains is presented in Fig. 8. The hydride strains during cooling in the RD are presented in Fig. 9.

As the hydrides start to precipitate at $T_p = 340$ °C they are under considerable compression (strain $\varepsilon = 10 \times 10^{-3}$). This compressive strain rapidly decreases as the temperature decreases, possibly because of change of shape and formation of dislocations that relieve the stress. At 320 °C the strain actually becomes positive, meaning that these hydride planes are now in *tension*. Thus, it is likely that between 340 °C and 320 °C considerable lattice plastic deformation occurs, as part of the hydride nucleation process. Once that is complete, the hydride strain remains approximately constant until 150 °C, which would be consistent with a plate lateral growth process occuring in the hydride plate in that temperature regime. In contrast, the strain in the RD is negative during the entire precipitation and cool-down process as shown in Fig. 9. This is likely because the diffracted intensity of the hydride planes in the RD come from the *edges* of the hydride platelets, in contrast to those planes observed in the TD which come from the *faces* of the reoriented hydride platelets.

It is also possible that this high compressive strain which is a diffraction peak shift observed when hydride first nucleate could be partly due to the initially forming hydrides having a slightly different stoichiometry than the Zr/H ratio of 1.66 typical in the δ-hydride

phase. Within the δ-hydride phase, a maximum change in *d*-spacing due to stoichiometry of 0.002 nm could lead to a pseudo-strain of 4000 microstrain [27,28]. Thus, the shift of hydride *d*-spacing due to stoichiometry changes could account for some of the compressive strains observed although not all of the peak shift can be explained by this phenomenon.

The strains in both directions are in general quite reproducible from cycle to cycle, indicating that the increasing connectivity shown in the hydride morphology paragraph does not significantly affect on the hydride strains during precipitation. However, Fig. 8 shows that in the TD the hydride strains on the reoriented hydride faces increases with the number of thermo-mechanical cycles. This is likely linked to the increase in reoriented hydride fraction with the increased number of cycles. More reoriented hydrides with their TD faces are present with an increasing number of cycles so the average strain of the entire hydride population increases as well.

Figs. 10 and 11 show the hydride strains in the TD and the RD, respectively, during heating. These heating curves are noticeably different for different cycles. In the first cycle (Fig. 10) the hydride strain increases due to thermal expansion. In the TD for the 2nd and 4th cycle, heating will dissolve hydrides that were initially in tension because they are reoriented. Therefore heating relaxes and reduces the tensile strains in the hydride. For the heating curve of the 1st cycle, compressed circumferential hydrides are dissolving. Therefore heating relaxes those compressive hydride strains. It can be seen that just before complete dissolution for hydrides in the TD and the RD, the strains are typically close to zero, which confirms the hypothesis that the hydride strain at high temperature is close to the unstressed value. In Figs. 10 and 11 and for all cycles, the change in the hydride strain regime during dissolution is seen around 350 °C which is similar to the change observed during precipitation.

For the planes oriented in the RD heating also relaxes the hydrides but since they started in a compressive state in this direction, no change is seen after the 1st cycle. The cooling curves for these strains in subsequent cycles are very similar to those seen in the 1st cycle. A clear difference is observed in the 4th cycle when the hydrides are unloaded and cooled to room temperature. As hydrides are cooled from 150 °C to room temperature, the strain in the TD is constant with temperature whereas the strain in the RD decreases with temperature in a manner similar to the strain evolution in non-reoriented hydride platelets. This confirms the hypothesis that the signal from hydride planes in the TD comes from reoriented hydride platelet *faces*, while the signal in the RD comes from non-reoriented hydride platelet *edges*.

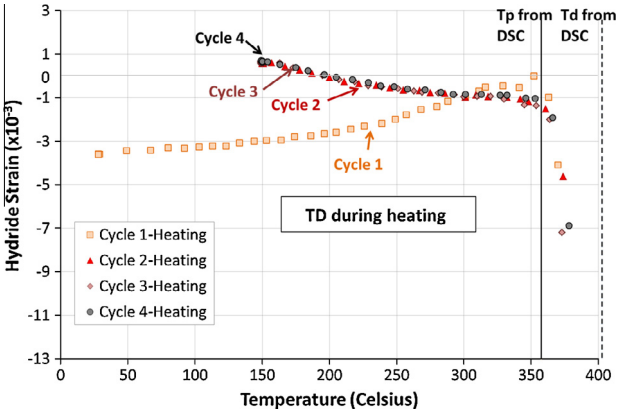

Fig. 10. Strain of hydride (1 1 1) peak in the TD in a sample with 192 wt.ppm of hydrogen during heating for four cycles under a 230 MPa applied stress (stress applied in the TD, full reorientation of hydrides).

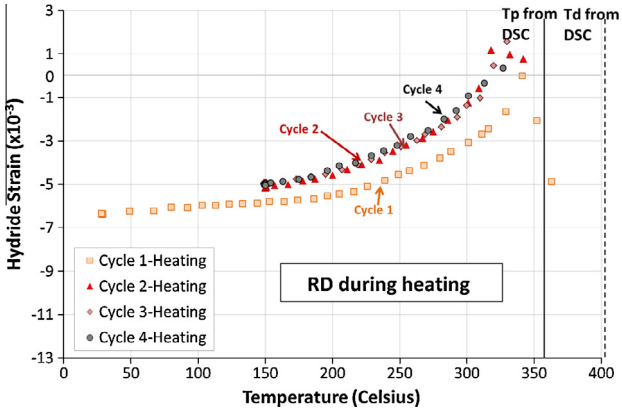

Fig. 11. Strain of hydride (1 1 1) peak in the RD in a sample with 192 wt.ppm of hydrogen during heating for four cycles under a 230 MPa applied stress (stress applied in the TD, full reorientation of hydrides).

3.4. Hydride peak broadening

The third parameter analyzed by the fitting of the diffraction peaks is the peak width or full-width at half-maximum (FWHM). The FWHM is influenced by the size of the particles considered or by the strain distribution in the particle population. For the hydride peaks considered here, the peak broadening has been previously determined to be caused mostly by *strain* broadening, very soon after the hydride particles have started precipitating [7,15,22].

Fig. 12 shows the overall evolution of the FWHM of δ{1 1 1} hydride peaks in both RD (circles) and TD (squares) with temperature and cycles. These results come from the same sample discussed above and show that the FWHM is high at elevated temperature, decreasing to a final value of the FWHM of TD planes upon reaching 150 °C with increasing number of cycles. The partial reorientation signature described in [15] showed that when sampling a hydride population with different orientations (in this case a mixed population of circumferential and radial hydrides) the hydride FWHM in the tensile stress direction would increase continuously during cool-down. The hydride peak FWHM in the direction perpendicular to the tensile stress however remain constant upon cool-down. This partial reorientation signature is observed in the first cycle in the TD in Fig. 12. For the following cycles, as hydrides progressively align to a fully reoriented state under tensile load the hydride FWHM in the TD decreases.

In the 4th cycle, when hydrides are cooled to room temperature under no stress, the FWHM in the TD increases. This could be due to the fact that reoriented hydrides have greater difficulty accommodating to the thermal contraction of neighboring zirconium grains compared to circumferential hydrides.

3.5. Summary of findings

This study showed that the threshold stress for hydride reorientation did not vary with hydrogen content and number of cycles, although increasing number of cycles strongly increased the reoriented hydride fraction and changed hydride morphology (size and connectivity). With increasing number of cycles the radial hydride fraction increases and the hydrides become larger and more connected. Both of these effects lead to increased probability of cladding failure. An increase in hydrogen content results in a smaller fraction of reoriented hydrides but an equivalent radial hydride content when full dissolution is achieved which could means there are a limited number of sites favorable for radial hydride nucleation.

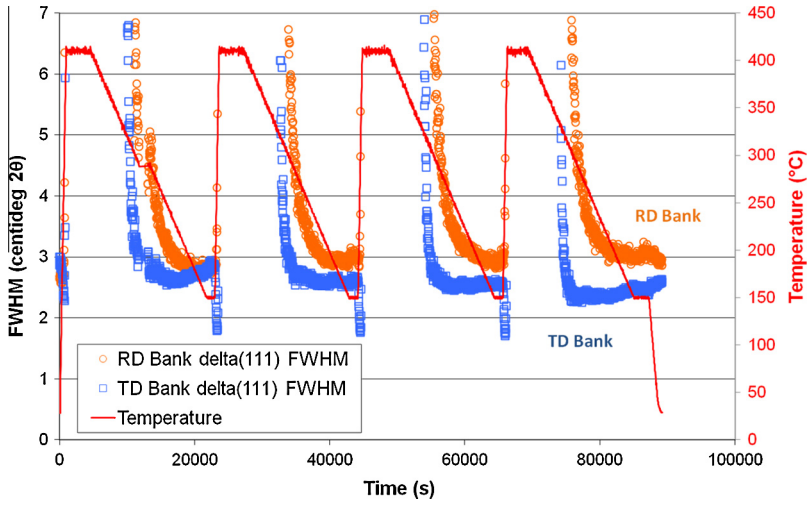

Fig. 12. FWHM as a function of time for hydride (1 1 1) peak in the TD and the RD in a sample with 192 wt.ppm of hydrogen cooled under a 230 MPa applied stress (stress applied in the TD, full reorientation of hydrides).

In situ X-ray diffraction has been used to study the kinetics of hydride dissolution and precipitation. The activation energy for the hydrogen precipitation of *reoriented* hydrides is lower than that of *circumferential* hydrides. This suggests that stress acts to suppress circumferential hydride precipitation thus enabling hydrides to precipitate in a different orientation. The dissolution and precipitation temperatures are not affected by the number of thermal cycles.

The effect of thermal cycling under load on elastic strains measured from the *d*-spacing shifts of zirconium matrix planes is small. In contrast the effect of cycling on the hydride strains, although small, is more noticeable. In particular, during hydride dissolution, planes in tension in reoriented hydrides (in the TD) and in compression on the edges of hydrides (in the RD) relax progressively to a zero strain value. This supports the idea that the high temperature value for the hydride *d*-spacing just before full dissolution is a valid unstressed value. The strain behavior in the TD and the RD during cooling is similar for all cycles while the load is on, although the higher magnitude of the hydride strains in the TD with increasing number of cycles could be linked to the increase of the RHF.

When the load is removed and the sample is cooled fast to room temperature, the strain behavior for reoriented hydrides is very different than for circumferential ones. Reoriented hydrides seem to be unfavorably oriented to accommodate for thermal contraction of local zirconium grains compared to circumferential hydrides. This behavior is seen in all cycles where hydride reorientation was observed.

4. Conclusions

The main conclusions of the study of the effect of thermo-mechanical cycling on hydride microstructure and strains in CWSR Zircaloy-4 are summarized below:

1. Cycling under stress above the threshold stress for reorientation drastically increases both the reoriented hydride fraction and the hydride size. The reoriented hydride fraction decreases with increasing hydrogen content although the radial hydride content remains constant (for levels above 200 wt.ppm).
2. The precipitation of *reoriented* hydrides under stress above the threshold stress for reorientation occurs at a lower temperature than the precipitation of in-plane (circumferential) hydrides in unstressed samples. The effects of cycling on the precipitation temperature when precipitating reoriented hydrides are small.
3. When radial hydrides precipitate under stress, during the first precipitation stage at high temperature the hydride strains become tensile in the direction perpendicular to the hydride platelet face. During the second precipitation regime, these strains remain constant in tension. This indicates a different hydride strain state for reoriented hydrides than for circumferential hydrides.
4. The magnitude of the tensile hydride strain in the transverse direction as measured by the change in *d*-spacing in the reoriented hydride face increases with cycling, potentially because of the increasing reoriented hydride fraction.
5. The analysis of the FWHM confirms the observed 'signature' of hydride reorientation in a mixed population of hydrides as previously observed in the literature. Once the hydride population is fully reoriented, the FWHM decreases due to the fact that a single population of reoriented hydrides is now present. The strain distribution in this single population is smaller than for a mixed population of circumferential and reoriented hydrides.

Acknowledgements

This research was funded by the Materials World Network Grant DMR-0710616 from the National Science Foundation, with corresponding funding from NSERC for the Canadian partners. We are grateful for their support. The research for this publication was supported by the Pennsylvania State University Materials Research Institute Nano Fabrication Network and the National Science Foundation Cooperative Agreement No. 0335765, National Nanotechnology Infrastructure Network, with Cornell University. Use of the Advanced Photon Source was supported by the U.S. Department of Energy, Office of Basic Energy Sciences under Contract No. DE-AC02-06CH11357. We would like to thank the 'Commissariat à l'Energie Atomique-CEA/DMN' for the use of the Hydromorph CEA Code for image analysis of the hydrides.

References

[1] C. Lemaignan, A.T. Motta, in: R.W. Cahn, P. Haasen, E.J. Kramer (Eds.), Materials Science and Technology A Comprehensive Treatment, VCH, New York, 1994, pp. 1–51.
[2] J.J. Kearns, C.R. Woods, J. Nucl. Mater. 20 (3) (1966) 241–261.
[3] A. Racine, PhD dissertation, Ecole Polytechnique, Palaiseau, France, 2005.
[4] M.C. Billone, T.A. Burtseva, R.E. Einziger, J. Nucl. Mater. 433 (2013) 431–448.
[5] C.E. Ells, J. Nucl. Mater. 35 (3) (1970) 306–315.

[6] M. Aomi, T. Baba, T. Miyashita, K. Kamimura, T. Yasuda, Y. Shinihara, T. Takeda, J. ASTM Int. 5 (9) (2008).
[7] K.B. Colas, A.T. Motta, J.D. Almer, M.R. Daymond, M. Kerr, A.D. Banchik, P. Vizcaino, J.R. Santisteban, Acta Mater. 58 (2010) 6565–6583.
[8] O. Zanellato, M. Preuss, J.-Y. Buffiere, F. Ribeiro, A. Steuwer, J. Desquines, J. Andrieux, B. Krebs, J. Nucl. Mater. 420 (2012) 537–547.
[9] M. Kerr, PhD dissertation, Queen's University, Kingston, ON, Canada, 2009.
[10] M. Kerr, M.R. Daymond, R.A. Holt, J.D. Almer, J. Nucl. Mater. 380 (1–3) (2008) 70–75.
[11] P.A.C. Raynaud, D.A. Koss, A.T. Motta, J. Nucl. Mater. 420 (2012) 69–82.
[12] T.M. Link, D.A. Koss, A.T. Motta, Nucl. Eng. Des. 3 (1998) 379–394.
[13] K.B. Colas, PhD dissertation, The Pennsylvania State University, University Park, 2012.
[14] V. Perovic, G.C. Weatherly, C.J. Simpson, Acta Metall. 31 (9) (1983) 1381–1391.
[15] K.B. Colas, A.T. Motta, M.R. Daymond, M. Kerr, J.D. Almer, J. ASTM Int. 8 (1) (2011).
[16] A.C. Larson, R.B.V. Dreele, GSAS, Los Alamos National Laboratory, 2000.
[17] P.A.C. Raynaud, PhD dissertation, The Pennsylvania State University, University Park, 2009.
[18] J. Bai, J. Gilbon, C. Prioul, D. Francois, Metall. Mater. Trans. A (1994) 25.
[19] D. Hardie, M.W. Shanahan, J. Nucl. Mater. 55 (1) (1975) 1–13.
[20] R.S. Daum, S. Majumdar, Y. Liu, M.C. Billone, Water Reac. Fuel Perf. Meet, Kyoto, Japan, 2005.
[21] K. Une, S. Ishimoto, J. Nucl. Mater. 322 (1) (2003) 66–72.
[22] K.B. Colas, A.T. Motta, M.R. Daymond, J.D. Almer, in: Zirc. in the Nuc. Ind.: 17th Int. Symp., ASTM, Hyderabad, India, 2013.
[23] J.J. Kearns, J. Nucl. Mater. 27 (1968) 64–72.
[24] A. McMinn, E.C. Darby, J.S. Schofield, Zirc. in the Nuc. Ind.: 12th Int. Symp., ASTM STP 1354, 2000, pp. 173–195.
[25] G.J.C. Carpenter, J.F. Watters, J. Nucl. Mater. 73 (2) (1978) 190–197.
[26] The Powder Diff. File, International Center for Diffraction Data, 2006.
[27] E. Zuzek, J.P. Abriata, A. San-Martin, et al., A. Int. Editor, Ohio, 2000, pp. 309–322.
[28] S. Yamanaka, K. Yamada, K. Kurosaki, M. Uno, K. Takeda, H. Anada, T. Matsuda, S. Kobayashi, J. Alloys Comp. 330–332 (2002) 99–104.